Molecular-orbital Studies on Carbametallaboranes. Part 3.† Tricapped Trigonal Prismatic Carbaplatinaborane and Related Polyhedral Molecules

By **D. Michael P. Mingos,*** Inorganic Chemistry Laboratory, University of Oxford, South Parks Road, Oxford OX1 3QR
Alan J. Welch, Department of Chemistry, The City University, London EC1V OHB

Extended Hückel molecular-orbital calculations are reported for the trigonal prismatic platinaboranes and carbaplatinaboranes $[B_8\{Pt(PH_3)_2\}H_8]^{2-}$ and $[B_6C_2\{Pt(PH_3)_2\}H_8]$, and the observed conformations of these molecules have been accounted for in terms of the nodal characteristics of the frontier orbitals of the constituent $Pt(PH_3)_2$ and carbaborane fragments. A description of the bonding in the less symmetrical isomer of $[B_6C_2\{Pt(PH_3)_2\}H_8]$ has been similarly derived from an analysis of the effect of transforming *nido*-$[B_8H_8]^{2-}$ into *arachno*-$[B_8H_8]^{2-}$.

In recent years the synthesis of a wide range of polyhedral carbametallaboranes by Hawthorne,[1] Grimes and co-workers,[2] and Stone [3] has given rise to a new and rapidly expanding area of organometallic chemistry. The development of new synthetic routes to these compounds has been accompanied by the development of a set of simple rules which can generally be used to account for the polyhedral geometries adopted by these molecules.[4,5] The serules cannot, however, be used to describe the more subtle structural aspects of carbametallaborane compounds, *e.g.* substitution patterns and conformational aspects. In order to provide a more flexible theoretical framework which would account for the detailed chemical and structural properties of these molecules we have initiated a programme of extended Hückel molecular-orbital calculations on the carbaplatinaboranes $[Pt(PH_3)_2C_nB_{x-n}H_x]^{(2-n)-}$ ($n = 1$ or 2; $x = 11$, 9, or 8). In former papers [6-8] the conformations and 'slip' distortions of the icosahedral carbametallaboranes have been discussed. This paper reports the extension of the basic principles developed in the previous papers to nine-vertex polyhedra.

Stone and co-workers [9] have shown that the reaction of $[Pt(stil)L_2]$ (stil = *trans*-stilbene, L = PMe_3 or PEt_3) with *closo*-1,6-R_2-$C_2B_6H_6$ (R = H or Me) affords two isomeric products. The structure of the major product

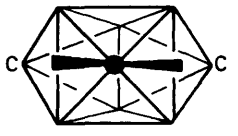

(1)

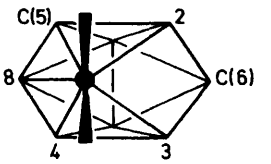

(2)

(1) may be described as a tricapped trigonal prism [10] with the two carbon atoms and the platinum atom occupying capping sites, whilst the minor product has the more open polyhedral geometry [11] shown in (2). In (2) the cage geometry closely resembles that found in B_8H_{12} (3) and may be derived from the bicapped trigonal prismatic geometry of the ligand (4) by a simultaneous lengthening of the B(2)–B(3) and B(4)–B(5) bonds. The metal is attached to the polyhedron in (2) by two short [B(4) 2.19, C(5) 2.19 Å] and three long [B(8) 2.56, B(2) 2.52, and B(3) 2.45 Å] bonds and therefore the linkage may be described as distorted η^5. The conformation of the PtL_2 fragment relative to the cage is quite different for (1) and (2) and a rotation of the PtL_2 plane by *ca.* 90° appears to be associated with the opening of the cage. Although the skeletons of (1) and (2) are related by relatively simple geometric changes, *i.e.* the simultaneous breaking of the B(2)–B(3) and B(4)–B(5) bonds and a rotation of the PtL_2 fragment, the activation energy for the process appears to be rather large. N.m.r. studies have indicated that (1) and (2) do not exchange to any appreciable extent up to temperatures of 70 °C, and the

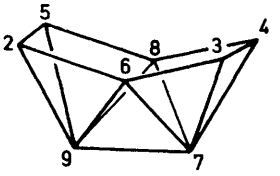

(3)

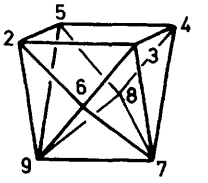

(4)

different positions taken up by the carbon atoms in the polyhedra also suggest the absence of a common low-energy intermediate.[12]

The following strategy has been used to understand the bonding in these complexes. The molecular orbitals of the bicapped trigonal prismatic $[B_8H_8]^{2-}$ polyhedron (4) were generated and then the effects of distorting this polyhedron to generate the open *arachno* cage structure shown in (3) were evaluated. The interactions between these polyhedra and the PtL_2 fragment were then considered. The influence of the carbon substituents was then regarded as a perturbation of the general bonding scheme so developed.

DETAILS OF CALCULATIONS

All calculations were based on the extended Hückel approximation [13] and the parameters used are identical with

† Part 2 in this series is ref. 8.

those reported previously.[6] The borane and carbaborane polyhedra were idealised and constrained to the following bond lengths: B–B = B–C = 1.78 Å, B–H = C–H = 1.2 Å.[10,11] The hydrogen atoms were positioned in such a way that the B–H (or C–H) vectors pointed towards the origin of the polyhedron. The $Pt(PH_3)_2$ fragment was assumed to have C_{2v} symmetry and was linked to the borane skeleton by bonds of length 2.200 Å.

1. nido-$[B_8H_8]^{2-}$ (4).—The bonding skeletal molecular orbitals (m.o.s) of the *nido*-$[B_8H_8]^{2-}$ ligand may be derived from the skeletal molecular orbitals of the parent trigonal prismatic $[B_6H_6]^{2-}$ ion using the capping principle which we have discussed previously.[14] Figure 1 illustrates the

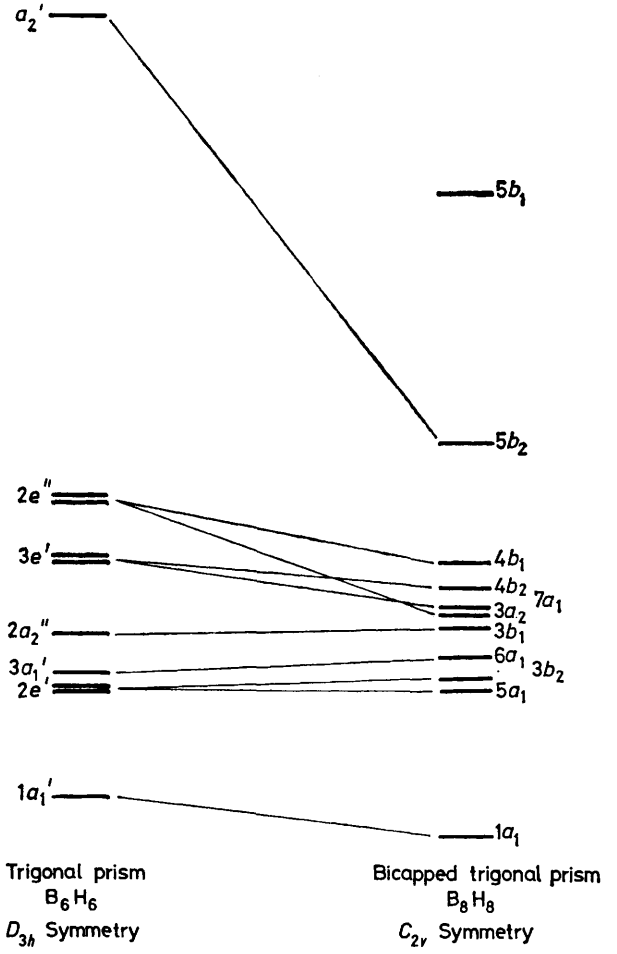

FIGURE 1 Molecular-orbital correlation diagram for the capping process: B_6H_6 (trigonal prism) + 2BH ⟶ B_8H_8 (bicapped trigonal prism). In B_8H_8 the ordering of the molecular orbitals is $5b_1 < 5b_2 < 4b_1 < 4b_2 < 7a_1 < 3a_2 < 3b_1 < 6a_1 < 3b_2 < 5a_1 < 1a_1$

relationship between the molecular orbitals of these related species and confirms that the *nido*-$[B_8H_8]^{2-}$ ion will have in common with its parent nine bonding skeletal m.o.s. The h.o.m.o.–l.u.m.o. (h.o.m.o. = highest occupied molecular orbital, l.u.m.o. = lowest unoccupied molecular orbital) separation is smaller however in the capped polyhedral ion because of the two low-lying virtual orbitals ($5b_2$ and $5b_1$ in Figure 1).

The ligating properties of the $[B_8H_8]^{2-}$ moiety will be decided primarily by those m.o.s which are localised predominantly on the open square face of the ligand and have energies and orbital characteristics which lead to strong interactions with the frontier orbitals of the $Pt(PH_3)_2$ fragment. The relevant molecular orbitals are illustrated schematically in Figure 2. A previous analysis [6] of the bonding in $[Pt(PH_3)_2(B_{11}H_{11})]^{2-}$ drew heavily on the similarity of the frontier m.o.s of $[B_{11}H_{11}]^{2-}$ and those of the cyclopentadienyl anion. The frontier orbitals of $[B_8H_8]^{2-}$ shown in Figure 2 indicate that such a simple analogy with cyclobutadiene is not valid. On the right-hand side of Figure 2 the familiar π m.o.s of C_4H_4 and their symmetry characteristics in the C_{2v} point group are indicated. The a_1 and a_2 m.o.s can be correlated with $7a_1$ and $3a_2$ of $[B_8H_8]^{2-}$ but the non-bonding b_1 and b_2 molecular orbitals derived from the e set of cyclobutadiene correlate with pairs of molecular orbitals of $[B_8H_8]^{2-}$, *i.e.* $4b_1$, $5b_1$ and $4b_2$, $5b_2$, which correspond to *in-phase* and *out-of-phase* combinations of the facial orbitals of $[B_8H_8]^{2-}$ with the p orbitals of the capping atoms.

2. arachno-$[B_8H_8]^{2-}$ (3).—Figure 3 illustrates schematically how the energies and radial characteristics of the frontier molecular orbitals of *nido*-$[B_8H_8]^{2-}$ are modified when the B(2)–B(3) and B(4)–B(5) bonds are simultaneously lengthened to generate the *arachno*-B_8H_8 skeleton. C_{2v} symmetry is maintained throughout this distortion mode and therefore the correlation of levels is a straightforward

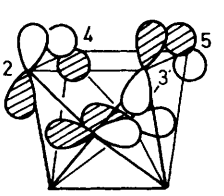

$4b_1$

(5)

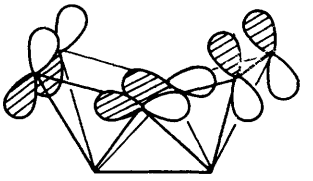

$4b_1$

(6)

process. The slopes of the correlation lines in Figure 3 can be readily understood in terms of the relative signs of the atomic orbital coefficients across the bonds which are being broken. The molecular orbitals of b_1 and a_2 symmetry, which have nodal planes passing through these bonds, are stabilised whilst the m.o.s of a_1 and b_2 symmetry, which have no such nodal planes, are destabilised. The different slopes of the $4b_1$, $4b_2$ and $5b_1$, $5b_2$ orbital pairs can be understood in terms of the additional contributions from the p orbitals on the capping atoms. For example, the $4b_1$ molecular orbital is antibonding between atoms 2 and 3 and between 4 and 5, but bonding with respect to the relevant capping atom [see (5)]. When the polyhedron is opened up the stabilisation resulting from the reduced overlap between the p orbitals on atoms 2 and 3 is, in part, offset by the reduced bonding interaction with the facial p orbital as shown in (6). The fact that the capping atom's p orbital is antibonding with respect to the facial atoms for the $5b_1$ molecular orbital (7) introduces an extra stabilising effect when the polyhedron is distorted [as shown in (8)].

The correlation diagram in Figure 3 clearly indicates that virtual orbitals of the two polyhedral borane fragments have different level orderings. This has a profound influence on the conformations of the carbaplatinaboranes, and will be discussed in more detail below. The correlation diagram

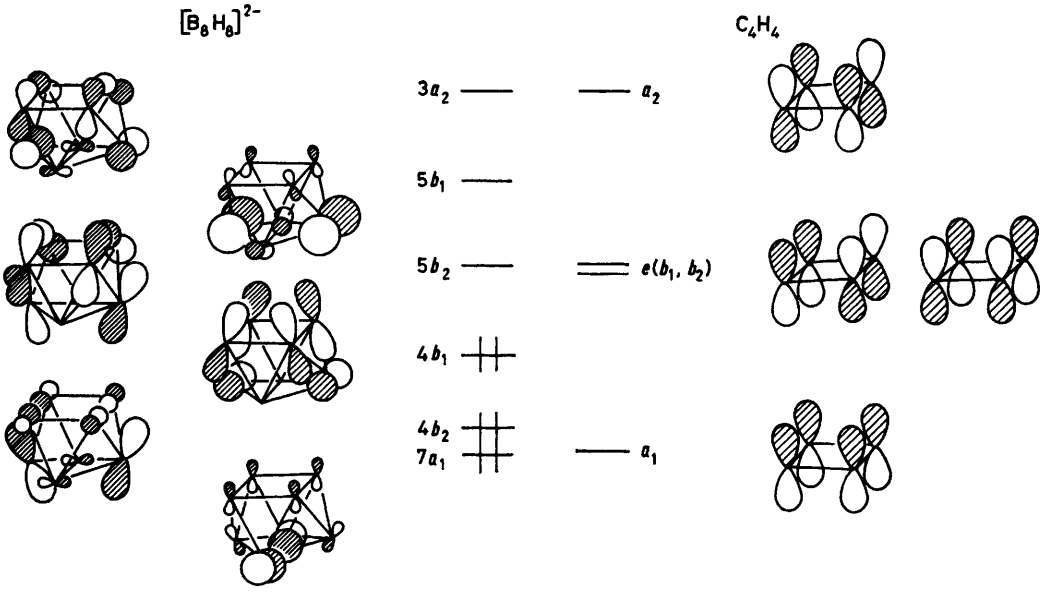

FIGURE 2 A comparison of the frontier molecular orbitals of $[B_8H_8]^{2-}$ and cyclobutadiene, C_4H_4

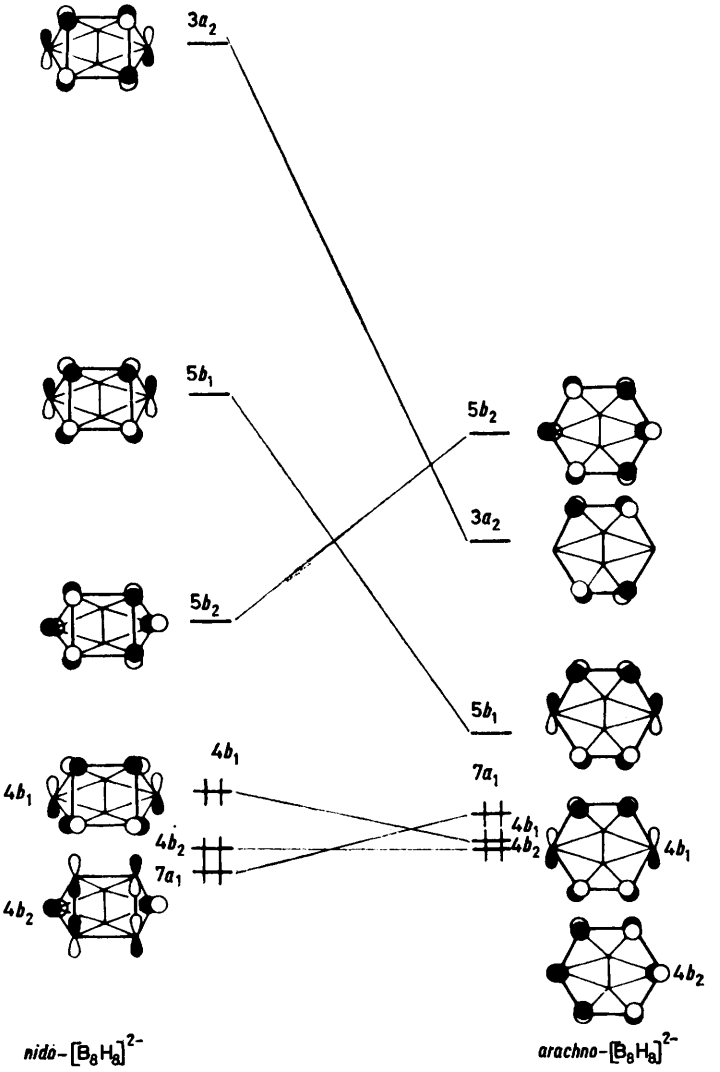

FIGURE 3 Molecular-orbital correlation diagram for the interconversion of *nido*-$[B_8H_8]^{2-}$ (C_{2v} symmetry) and *arachno*-$[B_8H_8]^{2-}$

also suggests that the interconversion of the *nido* and *arachno* polyhedral forms is an *allowed* process [15] for the $[B_8H_8]^{2-}$ ion, but a *forbidden* process for $[B_8H_8]^{4-}$, because in the latter the highest occupied $5b_2$ level of the *nido* polyhedron correlates with a virtual orbital of the *arachno* polyhedron.

3. closo-$[Pt(PH_3)_2(B_8H_8)]^{2-}$ (1).—The electronic characteristics of the $Pt(PH_3)_2$ fragment have been discussed in

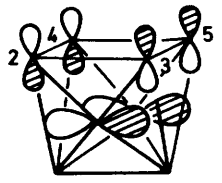

$5b_1$

(7)

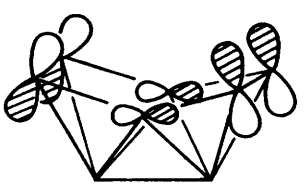

$5b_1$

(8)

some detail elsewhere [6] and it is only necessary for the present analysis to emphasise that the conformational preferences of this fragment are set by the frontier orbitals shown in Figure 4. The hybrid(xz) and yz orbitals are both occupied but do not have equal bonding capabilities. The more pronounced directional characteristics of the former give rise to larger overlap integrals with a target orbital of the correct symmetry. The acceptor orbitals of the fragment are the higher lying and empty hybrid(s)–(z) and y orbitals. The former is an s–p_z hybrid orbital of a_1 symmetry, and therefore its overlap integral with a m.o. on the

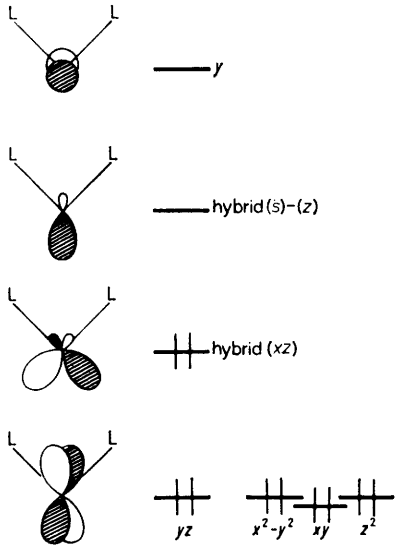

FIGURE 4 The frontier molecular orbitals for the $Pt(PH_3)_2$ fragment

$[B_8H_8]^{2-}$ ligand will be independent of the rotation angle, θ, which defines alternative conformations of the $[Pt(PH_3)_2(B_8H_8)]^{2-}$ complex. Rotational angles of θ = 0° and θ = 90° correspond to the more symmetrical, C_{2v}, possibilities shown in (9) and (10).

Our previous studies on the $Pt(PH_3)_2$ fragment have indicated that the most stable carbaplatinaborane conformation is achieved when the two-electron bonding interaction between the h.o.m.o. of the $Pt(PH_3)_2$ fragment, hybrid(xz), and the l.u.m.o. of the borane ligand is maximised. The *nido*-$[B_8H_8]^{2-}$ ligand has a l.u.m.o. of b_2 symmetry ($5b_2$ in Figure 3), and maximum hybrid(xz)–$5b_2$ overlap is achieved for the platinaborane conformation illustrated in (9) below. The hybrid(xz)–$5b_2$ interaction shown in (11) is more favourable than the alternative hybrid(xz)–$5b_1$ interaction (12) because the $5b_2$ orbital lies

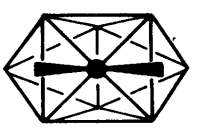

θ = 0°

(9)

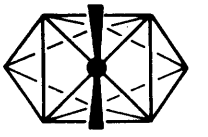

θ = 90°

(10)

some 3 eV closer in energy to hybrid(xz), and furthermore the $5b_2$–hybrid(xz) overlap intergral is larger than the $5b_1$–hybrid(xz) integral (see Table). Extended Hückel calculations have confirmed that this (θ = 0°) conformation (9) is more stable than that at θ = 90° by some 1.2 eV, and that the difference arises primarily from the different magnitudes of the interactions illustrated below. The calculations, however, also indicated significant interactions

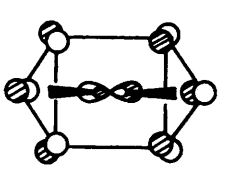

$5b_2$ - hybrid(xz)

(11)

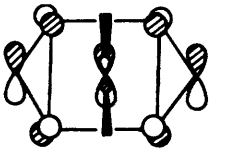

$5b_1$ - hybrid(xz)

(12)

between hybrid(xz) and the lower lying filled $4b_2$ orbital of the ligand, resulting from the appreciable $4b_2$–hybrid(xz) overlap integrals given in the Table. Although the $4b_2$–hybrid(xz) integral is smaller than the $5b_2$–hybrid(xz) integral, the $4b_2$–hybrid(xz) energy separation is smaller (see Figure 5). Therefore, we have the makings of a classical three-orbital bonding problem [16] which gives rise to bonding, non-bonding, and antibonding solutions. These

Interfragment overlap integrals for $Pt(PH_3)_2$ with *nido*-$[B_8H_8]^{2-}$

(*a*) θ = 0°			
⟨hybrid(xz)|$4b_2$⟩	0.1376	⟨hybrid(xz)|$5b_2$⟩	0.2551
⟨yz|$4b_1$⟩	0.1342	⟨yz|$5b_1$⟩	0.1264
(*b*) θ = 90°			
⟨hybrid(xz)|$4b_1$⟩	0.2185	⟨hybrid(xz)|$5b_1$⟩	0.2022
⟨yz|$4b_2$⟩	0.0890	⟨yz|$5b_2$⟩	0.1564

components can be clearly identified in Figure 5. The most stable orbital is the bonding orbital derived from the $4b_2$–hybrid(xz) interaction. The non-bonding component has almost equal contributions from hybrid(xz), $4b_2$, and $5b_2$, and may be visualised as the $5b_2$–hybrid(xz) bonding component (11) mixed with the (out-of-phase) $4b_2$ orbital as shown in (13) below. The non-bonding character is therefore achieved by a transfer of electron density from the facial to the capping atoms of the polyhedron.

The metal *yz* orbital also overlaps significantly with the $4b_1$ and $5b_1$ orbitals of the ligand (see Table), but the latter is so high-lying that significant $4b_1$, $5b_1$ mixing does not occur. Therefore, the *yz* orbital enters into what is

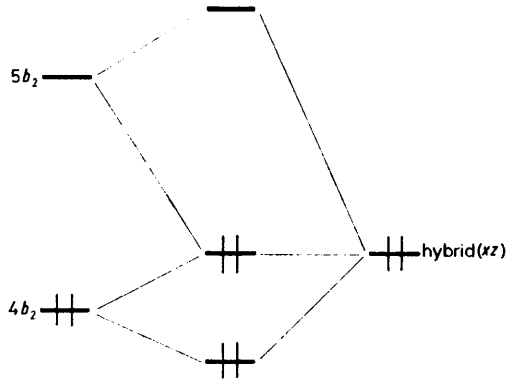

FIGURE 5 A simplified diagram of the interaction between the ligand $4b_2$ and $5b_2$ orbitals and the metal hybrid(*xz*) orbital

essentially a four-electron destabilising interaction with $4b_1$. The destabilising effect is mitigated slightly by the mixing in of the higher-lying metal orbital as illustrated in (14). A similar mixing phenomenon has been noted previously for $[Pt(PH_3)_2B_{11}H_{11})]^{2-}$.[6] When carbon atoms are substituted into the capping positions the C_{2v} symmetry of the molecule is retained and the molecular-orbital level orderings described above for $[B_8H_8]^{2-}$ are unchanged. Therefore, the

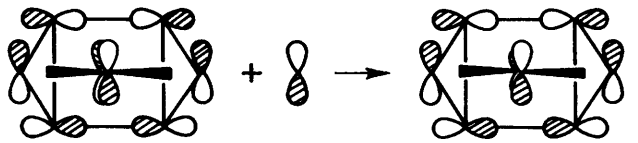

(14)

isoelectronic carbaborane complex $Pt(PH_3)_2(C_2B_6H_8)$ is predicted also to have the conformation illustrated in (9). Extended Hückel calculations on $Pt(PH_3)_2(C_2B_6H_8)$ have indicated that the barrier to rotation for the carbaborane complex might be slightly smaller than that for the parent borane complex because the $5b_2$–$5b_1$ energy separation is reduced. *X*-Ray crystallographic studies on two crystal forms of $1,1\text{-}(PMe_3)_2\text{-}6,8\text{-}Me_2\text{-}1,6,8\text{-}PtC_2B_6H_6$ have shown that the conformations of these complexes are close to that predicted by theory, the experimentally determined θ angles being *ca.* 12° in both forms.[10]

The calculated overlap populations for $Pt(PH_3)_2(C_2B_6H_8)$ are illustrated in (15) and suggest that the square face of the $C_2B_6H_8$ ligand will distort on co-ordination to the $Pt(PH_3)_2$ fragment. The *X*-ray crystal structure of $1,1\text{-}(PMe_3)_2\text{-}6,8\text{-}Me_2\text{-}1,6,8\text{-}PtC_2B_6H_6$ has confirmed this distortion [see (16)] which arises primarily from the higher electron population of the $4b_1$ orbital which has a nodal plane passing through the capping atoms [see (5) above].

It follows from the analysis given above that if the related osmium complex $Os(PH_3)_2(C_2B_6H_8)$, which has two fewer valence electrons, could be prepared, the h.o.m.o.–l.u.m.o. interactions would be maximised for the alternative conformer (10) where $\theta = 90°$. The extended Hückel calculations suggest that the conformer (10) will be more stable than (9) for the osmium complex by *ca.* 0.5 eV. For such a complex the m.o. illustrated in (14) is empty, and is ideally hybridised at the metal atom to act as an acceptor orbital for a small incoming ligand, *e.g.* CO. The resultant $Os(CO)(PR_3)_2(C_2B_6H_8)$ complex is, therefore, also predicted to be stable.

4. nido-$[Pt(PH_3)_2(B_8H_8)]^{2-}$.—The frontier molecular orbitals of the *arachno*-$[B_8H_8]^{2-}$ skeleton have been discussed above and it was noted that the generation of this polyhedral fragment from *nido*-$[B_8H_8]^{2-}$ results in dramatic changes in the relative order of the virtual molecular orbitals. In particular, Figure 3 shows that for the more open polyhedral cage the lowest lying molecular orbital is

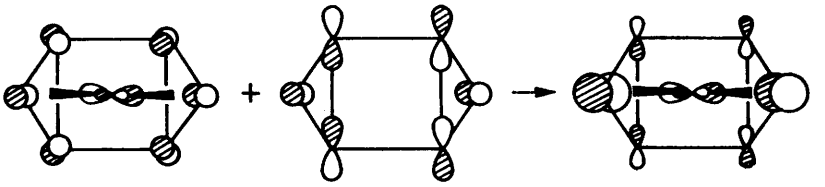

(13)

$5b_1$. This has clear implications regarding the conformation of the $Pt(PH_3)_2$ complex. The maximum hybrid(*xz*)–*arachno*-$[B_8H_8]^{2-}$ overlap will now be achieved when the rotation angle θ is equal to 90° [see (17)]. Extended Hückel calculations have confirmed that if the metal fragment is constrained to lie above the centre of the polyhedron this is the most stable conformation. In addition the calculations indicate the importance of mixing between the $4b_1$ and $5b_1$ levels in a sense which is analogous to that discussed above for the complex formed between *nido*-$[B_8H_8]^{2-}$ and $Pt(PH_3)_2$.

The presence of the low lying $3a_2$ level in the case of *arachno*-$[B_8H_8]^{2-}$ introduces an additional complication

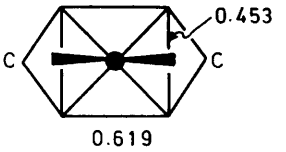

Overlap populations

(15)

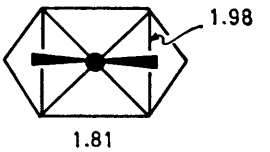

Bond lengths (Å)

(16)

which was not present for the *nido* polyhedron. For symmetry reasons the $3a_2$ m.o. has zero overlap with hybrid(*xz*) when the platinum atom lies above the centre of the

polyhedron. However, if the platinum atom is allowed to move along the mirror plane, with the translational distortion defined by Δ in (18) then $3a_2$ can enter into a bonding interaction with hybrid(xz) as shown below. In addition

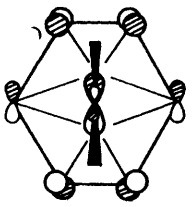

(17)

the four-electron destabilising interaction between yz and $4b_2$ is reduced by such a ' slip ' distortion. Extended Hückel calculations have confirmed that these new interactions are energetically favourable and predict a slipped geometry for this isomer.

The X-ray crystallographic analysis [11] of 1,1-$(PEt_3)_2$-5,6-Me_2-1,5,6-$PtC_2B_6H_6$ has shown that this isoelectronic carbaborane complex does indeed have a ' slipped ' geometry and a conformation close to that predicted above [see (2) above for an illustration of the conformation established by the crystallographic study]. In this carbaplatinaborane the carbon atoms are not symmetrically disposed with respect

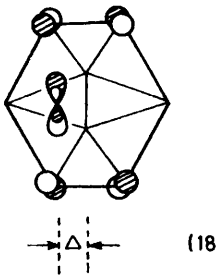

(18)

to the mirror plane and therefore the nodal characteristics of the important $5b_1$ level are altered by the substitution of the carbon atoms in a way which is illustrated schematically below in (19). The rotation of the nodal plane accounts for

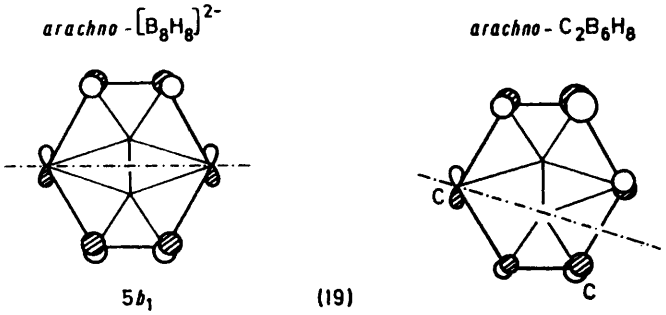

(19)

role in stabilising the carbaborane complex and in influencing its equilibrium conformation. An extreme view of this process has been recognised previously by Stone [3] and Wallbridge and co-workers [17] who have formulated these complexes as platinum(II) complexes of the $[C_2B_nH_{n+2}]^{2-}$ ligand. From Figure 3 it is clear that such a formulation leads to the population of the $5b_2$ level for *nido*-B_8H_8 and the $5b_1$ level for *arachno*-B_8H_8. As we have noted above the interconversion of the two polyhedral forms in such a situation will be a symmetry forbidden process, and will presumably have a high activation energy. Therefore, the observation that the two isomeric forms of $Pt(PMe_3)_2(C_2B_6H_8)$ do not readily interconvert [12] can be related directly to the bonding model which has been developed for these complexes. Furthermore, the analysis carries the clear implication that it might be possible to promote an interconversion of the isomeric forms photochemically.[15] It also

follows that the isomeric possibilities for the analogous osmium complex may interconvert much more readily, because they will have two fewer valence electrons.

The discussion up to this point has been limited to a consideration of the interconversion of *nido*- and *arachno*-$[B_8H_8]^{2-}$ through the simultaneous breaking of two opposite bonds in the polyhedral framework. If a bond is made only between the boron atoms 2 and 3 of the *arachno*-$[B_8H_8]^{2-}$ framework then an alternative $[B_8H_8]^{2-}$ *nido*-polyhedron is generated as illustrated below in (20).

The new polyhedron is also related to the tricapped trigonal prism, from which it can be generated by the removal of one of the non-capping vertices. Co-ordination of the

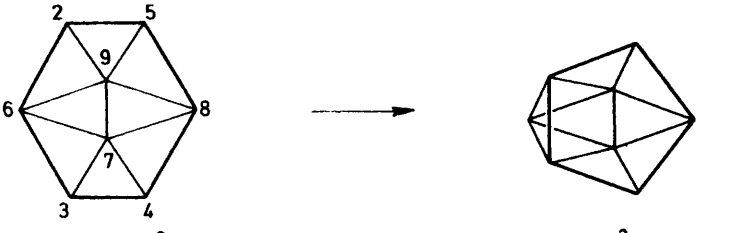

(20)

the slight rotation of the $Pt(PR_3)_2$ fragment observed in the X-ray crystallographic analysis [9,11] and illustrated in (2).

5. *Interconversion of the Isomers of* $[Pt(PH_3)_2(B_8H_8)]^{2-}$.— The discussion above has clearly indicated that the donation of electron density from the metal hybrid(xz) orbital to the lowest unoccupied level of the ligand plays an important

$Pt(PH_3)_2$ fragment to the open pentagonal face of this ligand would therefore generate an alternative isomer of the *closo*-metallaborane polyhedron $[Pt(PH_3)_2(B_8H_8)]^{2-}$.

Figure 6 illustrates the correlation diagram for the interconversion illustrated in (20), and the slopes of the m.o.s can be understood as before. The *arachno*-$[B_8H_8]^{2-}$ polyhedral

cage is the more stable largely because of the reduced antibonding characteristics of the $5b_1$ and $4b_1$ energy levels. The corresponding $Pt(PH_3)_2$ complex is also the more stable and as the interconversion is not a symmetry-forbidden process it is anticipated that even if the *closo* metallaborane or isoelectronic carbametallaborane complex were to form it would readily rearrange to the corresponding *nido* complex.

6. *Mechanism for the Formation of the Carbaplatinaboranes.*—The isomeric carbaplatinaboranes described above are generated in the following insertion reaction. It is not an unreasonable assumption that the first step in such a reaction is the generation of the co-ordinatively unsaturated and highly nucleophilic angular $Pt(PR_3)_2$ fragment, which subsequently attacks the carbaborane cage.

$$Pt(olefin)(PR_3)_2 + closo\text{-}1,6\text{-}C_2B_6H_8 \longrightarrow Pt(PR_3)_2(C_2B_6H_8) + olefin$$

Such an assumption has certain symmetry consequences which are worth exploring in order to understand, at least in a qualitative fashion, the distribution of isomeric products which result from the above reaction. The h.o.m.o. of the angular $Pt(PR_3)_2$ fragment will at this stage be familiar to the reader. Clearly this orbital will attempt to maximise its overlap with the l.u.m.o. of the *closo*-$1,6\text{-}C_2B_6H_8$ cage and thereby maximise the metal–carbaborane ligand charge transfer in the transition state. In (21) the major orbital contributions to the l.u.m.o. of $C_2B_6H_8$ are illustrated schematically. Following Hart and Lipscomb [18] we find that the l.u.m.o. of $1,6\text{-}C_2B_6H_8$ is concentrated predominantly on the symmetry related and four-connected boron atoms B(4) and B(8) (29% on each), and to a lesser extent on the carbon atoms C(1) and C(6) (11% on each). This molecular orbital lies at −8.5 eV and consequently is well matched in energy terms with the h.o.m.o. of the $Pt(PR_3)_2$ fragment. The next lowest-lying energy level of the cage occurs at −4.5 eV.

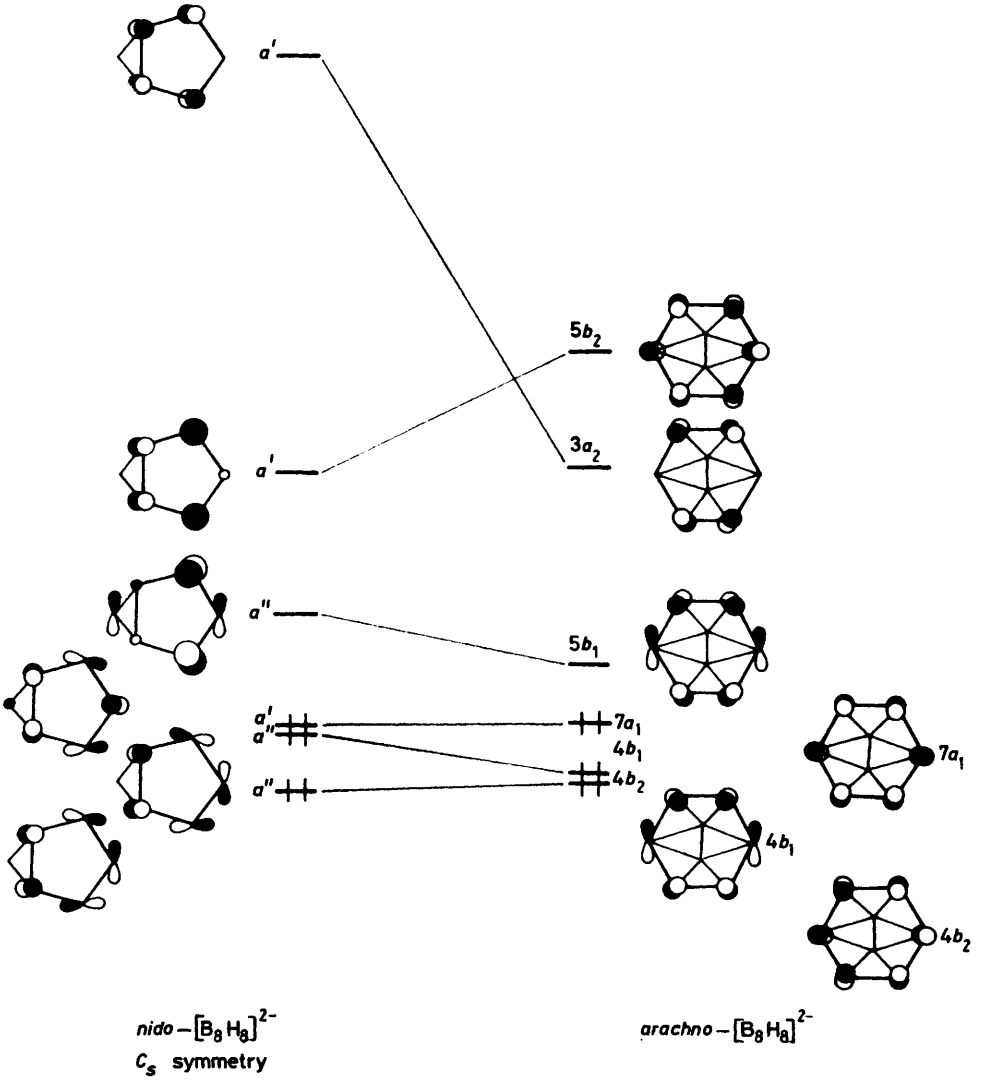

FIGURE 6 Molecular-orbital correlation diagram for the interconversion of *nido*-$[B_8H_8]^{2-}$ (C_s symmetry) and *arachno*-$[B_8H_8]^{2-}$

There are two distinct ways in which the metal fragment can approach the carbaborane cage and at the same time maintain the two-fold symmetry axis of the polyhedron. Approach of $Pt(PR_3)_2$ along the two-fold axis of the cage

towards the B(5)–B(7) edge as illustrated in (22) below will lead to the most effective overlap of the relevant metal and cage orbitals. If this interaction is followed by the fission

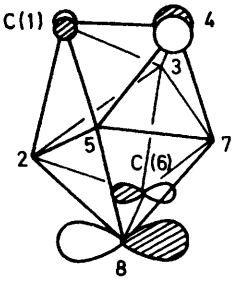

(21)

of the B(5)–B(7) bond then the resultant carbaplatinaborane is the isomer which is the major product of the reaction [*cf.* (1)]. Attack by the metal fragment along the two-fold axis but from the opposite direction towards the B(2)–B(3) edge would be far less favourable because the

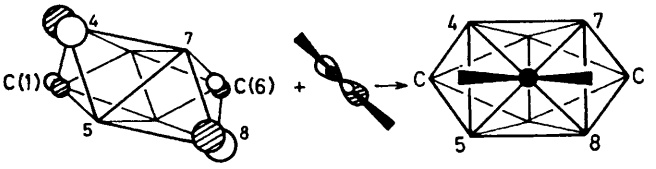

(22)

overlap between the metal h.o.m.o. and the C(1) and C(6) orbitals would be far less effective. The resultant carbaplatinaborane shown in (23) is not observed as a reaction product in agreement with the above analysis. The occurrence of the second isomer of $Pt(PR_3)_2(C_2B_6H_8)$ (2) is more

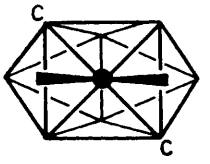

(23)

difficult to rationalise since its formation requires the breaking of three boron–carbon and boron–boron bonds in the parent *closo* borane. Approach of the $Pt(PR_3)_2$ fragment towards the B(2)–B(5) edge [or the symmetry related B(3)–B(7) edge] would be able to take advantage of a favourable overlap with the boron and carbon *p* orbitals subtending, for example, the B(3)–B(4)–B(7)–C(6) dome as shown in (24). Fission of the B(3)–B(4) and B(3)–B(7) bonds would lead to the carbaplatinaborane illustrated in

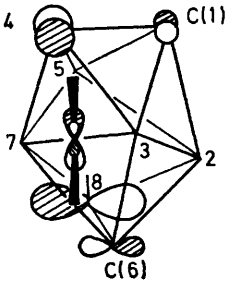

(24)

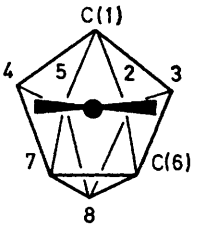

(25)

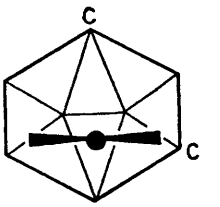

(26)

(25), which the theoretical analysis above has shown could rearrange to the observed isomer (26).

[9/1288 *Received*, 13*th August*, 1979]

REFERENCES

[1] M. F. Hawthorne, *J. Organometallic Chem.*, 1975, **100**, 97.
[2] D. C. Beer, V. R. Miller, L. G. Sneddon, R. N. Grimes, M. Mathew, and G. J. Palenik, *J. Amer. Chem. Soc.*, 1973, **95**, 3046.
[3] F. G. A. Stone, *J. Organometallic Chem.*, 1975, **100**, 257.
[4] K. Wade, *Adv. Inorg. Chem. Radiochem.*, 1976, **18**, 1.
[5] R. Mason and D. M. P. Mingos, *M.T.P. Internat. Rev. Sci. Phys. Sci. Ser.* 2, 1975, **11**, 121.
[6] D. M. P. Mingos, *J.C.S. Dalton*, 1977, 602.
[7] M. I. Forsyth, D. M. P. Mingos, and A. J. Welch, *J.C.S. Chem. Comm.*, 1977, 605.
[8] M. I. Forsyth, D. M. P. Mingos, and A. J. Welch, *J.C.S. Dalton*, 1978, 1363.
[9] M. Green, J. L. Spencer, F. G. A. Stone, and A. J. Welch, *J.C.S. Chem. Comm.*, 1974, 794.
[10] A. J. Welch, *J.C.S. Dalton*, 1976, 225.
[11] A. J. Welch, *J.C.S. Dalton*, 1977, 962.
[12] J. L. Spencer, unpublished work.
[13] R. Hoffmann, *J. Chem. Phys.*, 1963, **39**, 1397.
[14] M. I. Forsyth and D. M. P. Mingos, *J.C.S. Dalton*, 1977, 610.
[15] R. B. Woodward and R. Hoffmann, *Angew. Chem. Internat. Edn.*, 1970, **8**, 781.
[16] W. L. Jorgensen and L. E. Salem, ' The Organic Chemists' Book of Orbitals,' Academic Press, New York, 1973.
[17] H. M. Colquhoun, T. J. Greenhough, and M. G. H. Wallbridge, *J.C.S. Chem. Comm.*, 1976, 1019.
[18] H. Hart and W. N. Lipscomb, *Inorg. Chem.*, 1968, **7**, 1070.